CHAPTER IV
RESULTS AND DISCUSSION

4.1 Polyaniline

4.1.1 Synthesized Polyaniline Characterization

Elemental analysis of the synthesized emeraldine base (EB) form of polyaniline powder (PANI) gave C = 73.790%, H = 5.305%, N = 14.177% and residual = 6.729%. The chemical formula of EB provided the theoretical values of C = 79.56%, H = 4.97%, N = 15.47%. Thermal analysis data of EB in Figure 4.1 shows two step weight losses. The minimum weight loss ~4 wt% of the first step weight loss occurs around 60-100°C; it can be attributed to the release of free and bound water molecules (Li and Wan, 1999). The second step weight loss can be identified as the decomposition of PANI chain backbone which occured around 510°C. Then residual % weight loss is assigned to %O from water molecules amounted to 0.22 mole per repeat unit.

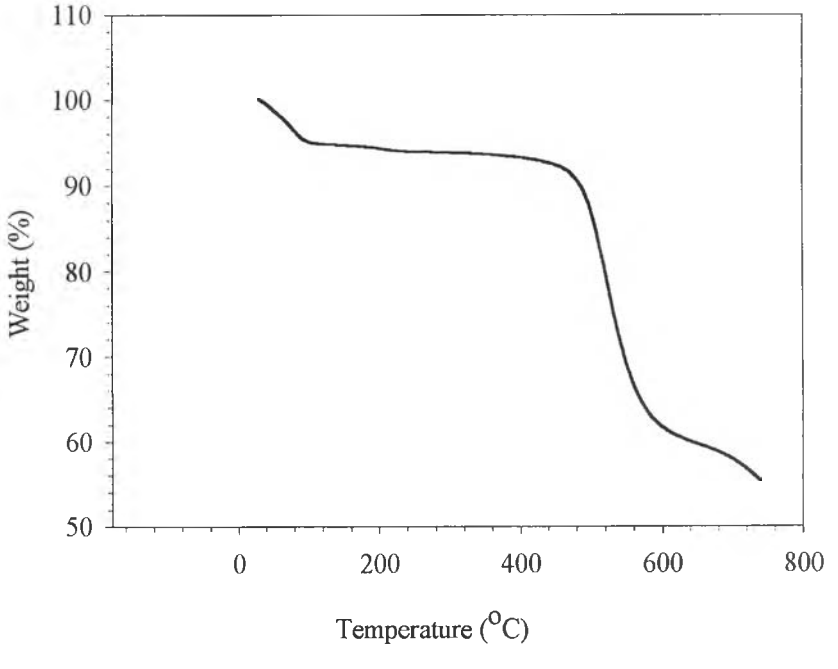

Figure 4.1 TGA thermogram of polyaniline emeraldine base under nitrogen atmosphere.

Figure 4.2 shows that the FT-IR spectrum of synthesized polyaniline having identical absorption peaks as found in the earlier studies (Salaneck, 1993, Zeng, 1998). The peak assignments of EB are summarized in Table 4.1.

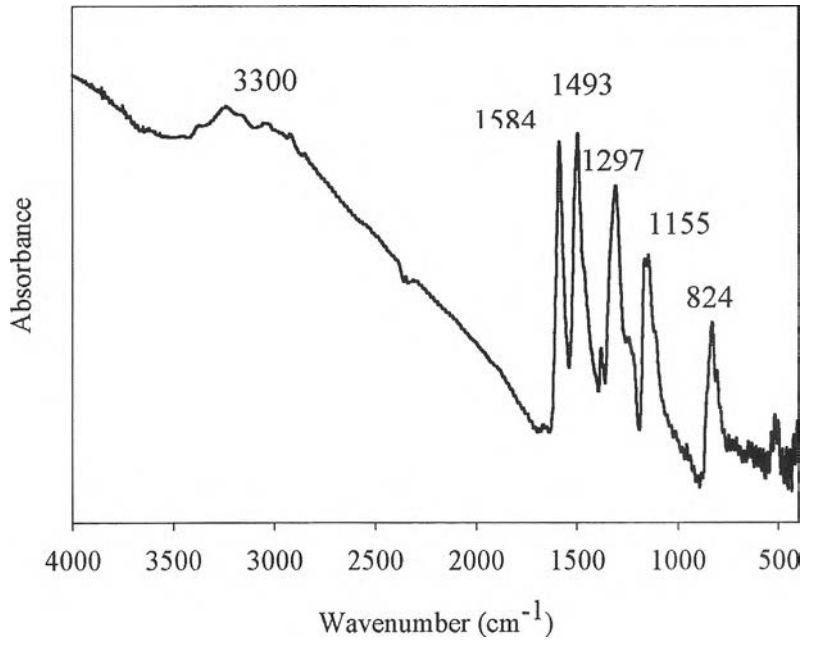

Figure 4.2 FT-IR spectrum of synthesized polyaniline emeraldine base.

Table 4.1 Function group of synthesized polyaniline emeraldine base (Salaneck, 1993 (1), Zeng *et al.*, 1998, (2))

Wavelength (cm^{-1})	Functional Group	Reference
3300	NH Stretching	1
1586	Stretching vibration of N-quinoid ring	1, 2
1493	Stretching vibration of N-benzenoid ring	1, 2
1297	Stretching vibration of C-N	1, 2
1161	vibration mode of quinoid ring	1, 2
825	C-H bending vibration of para-couple benzene ring	1, 2

Figure 4.3 shows that an UV-vis absorption spectrum of EB consisting of 2 absorption bands at 325 nm and 627 nm. They confirm the polyaniline structure. The peak at 325 nm can be assigned to the π-π^* transition in the polymer conjugated backbone or the transition across the band gap. The peak at 633 nm has been

assigned to the creation of a localized molecular excitation with an electron on a quinoid part and a hole on the neighboring two-benzenoid part (Duke, 1986, Huang, 1986 and McCall, 1989).

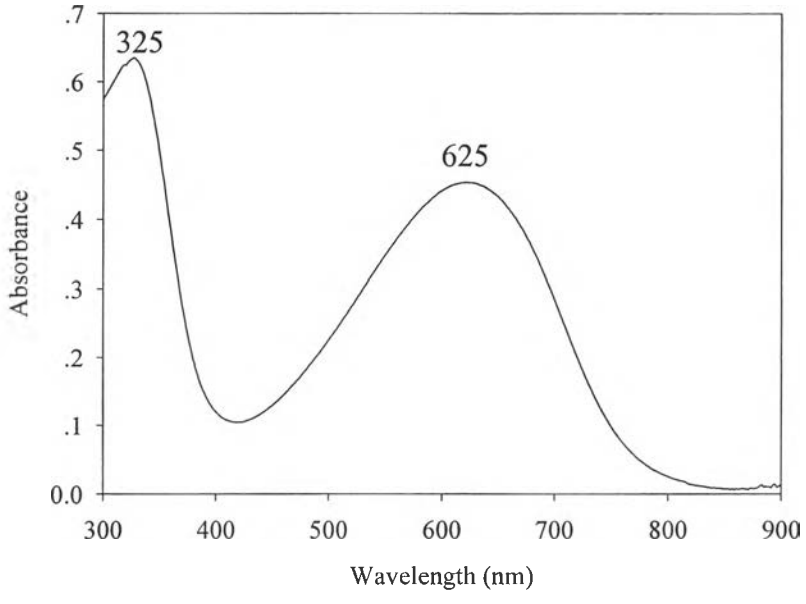

Figure 4.3 UV-vis spectrum of synthesized polyaniline emeraldine base in NMP solvent.

4.1.2 Acid-Doped Polyaniline Characterization

The electrical conductivity of polyaniline depends on two factors: namely the degree of oxidation of the polyaniline and the degree of protonation of the material. Unprotonated polyaniline base is an insulating material. The electrical conductivity is associated with the protonated form observed in polyaniline salt or acid-doped polyaniline.

4.1.2.1 Thermogravimetric analysis

Figure 4.4 shows the TGA themograms of an emeraldine base and acid-doped polyanilines using hydrochloric acid (PANI-HCl) and maleic acid (PANI-MA). The thermograms of acid-doped polyanilines show a three-step weight loss behavior. The first step can be attributed to the loss of water between 50-90°C. The second step weight loss is continuous from 190-250°C due to the loss of the dopants. The analytical results are listed in Table 4.2.

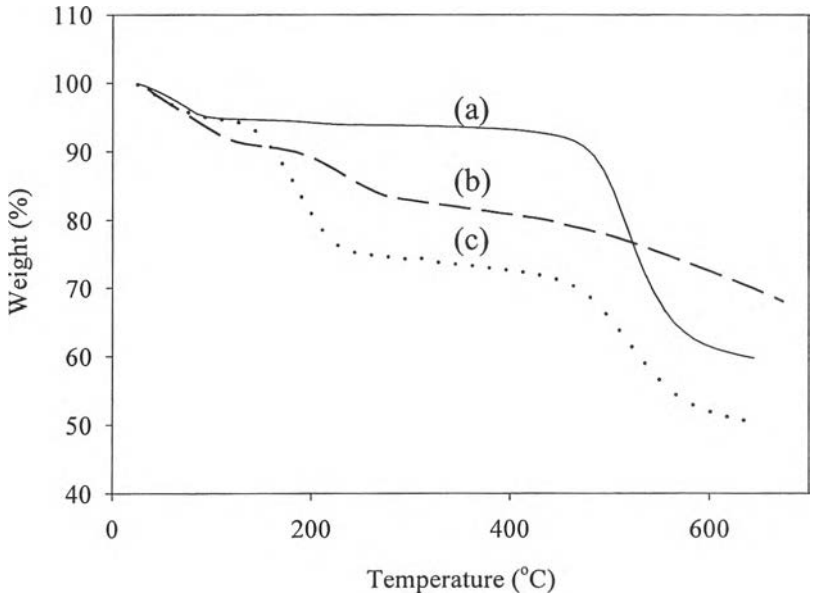

Figure 4.4 TGA thermograms of (a) an emeraldine base, (b) PANI-HCl at doping ratios = 1.0 (c) PANI-MA at doping ratios = 1.0.

Table 4.2 The TGA results of an emeraldine base and acid-doped polyaniline

Step loss	PANI-EB		PANI-HCl		PANI-MA	
	%loss	Onset (°C)	%loss	Onset (°C)	%loss	Onset (°C)
First-step	4 ± 0.2	100	12 ± 2	82 ± 5	4 ± 1	55 ± 5
Second-step	17	552	11 ± 1	220 ± 5	30 ± 2	192 ± 5
Third-step			15	537	17	538

The amount of weight loss due to evaporation of moisture for PANI-HCl (~12%) was greater than those of PANI-MA (~4%) and emeraldine base form (~4%). It slightly increased with doping level indicating that the HCl-doped polyaniline adsorbed water readily as shown in Figure 4.5.

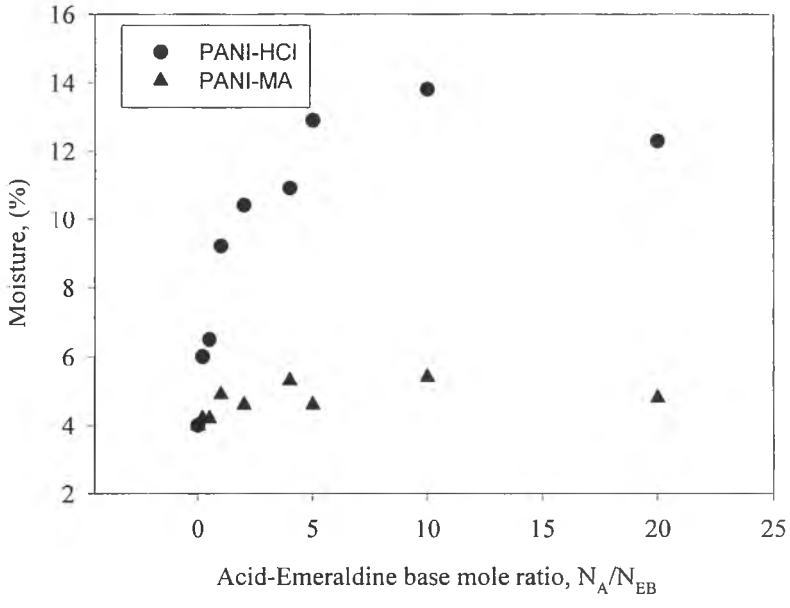

Figure 4.5 Moisture contents of PANI-HCl and PANI-MA powder at various doping ratios.

Matveeva *et al.* (Zeng *et al.*, 1998) reported that it is very difficult to remove the bound water completely by drying. Kahol *et al.* (1997) reported that a complete removal of water via pumping under a vacuum (about 10^{-4} torr) could not be accomplished. They also reported that water molecules were adsorbed at two sites of polyaniline chain: (i) on the positive charged part (=NH^+-) of the polymer backbone (N-site) and (ii) on dopant anions (X-site) at which water molecules were more strongly absorbed than those at N-site. Both experimental and theoretical studies revealed that the electrical behavior of polymer was sensitively dependent on moisture (Cowie, 1991). So all doped polyaniline powders used in experiment were vacuum dried 48 hours to remove as much as possible the moisture content and to minimize the effect of moisture on electrical conductivity. After fabricating polyanilines into pellets, they were kept in a dessicator to prevent additional moisture pick up for further use. The data on moisture content were used to calculate %oxygen from the elemental analysis data.

4.1.2.2 Elemental analysis

The effect of dopant on the doping level of the conductive polymer was studied by using an elemental analysis. In the protonation doping process of an emeraldine base (EB), the amount of protons from an acid dopant which protonates the nitrogen atoms in the polyaniline chain can be used to calculate the percentage of apparent doping level $\%[H]_{acid}/[N]$, as in Equation A1 and as explained in details in Appendix A

$$\%\text{Apparent doping level} = [H]_{acid}/[N] \times 100 \quad \text{(A.1)}$$

The percentage of apparent doping level could be converted to the percentage of doping level by multiplying by a factor of 2. The percentage of doping levels of PANI-HCl and PANI-MA powder at various acid-emeraldine base ratios, (N_A/N_{EB}) is shown in Table 4.3.

Table 4.3 Percentage of doping level of PAN-HCl and PANI-MA

N_A/N_{EB}	% Doping level of PANI-HCl	% Doping level of PANI-MA
EB	0	0
0.2	11.06	10.76
0.51	37.48	28.1
1.0	64.42	57.48
2.0	94.02	94.16
4.0	96.34	96.74
5.0	98.66	98.58
10.0	97.9	96.08
20.0	99.56	100.46

Figure 4.6 shows that the percentage doping level of PANI-HCl and PANI-MA powder vs acid-emeraldine base mole ratio. The percentage of doping level of PANI-HCl for N_A/N_{EB} less than 2 is higher than that of PANI-MA because HCl, strong acid, has a higher dissociation constant than that of MA and it can produce many protons to react with nitrogen atoms at the quinoid ring. At the mole ratio greater than 2, the effect of acid strength is no longer severe. It can be

seen from Table 4.3 that the percentage doping level nearly reaches the equilibrium of 100%. This suggests that 2:1 mole ratio of acid and emeraldine base (EB) is the ratio required to give a completely protonated polymer

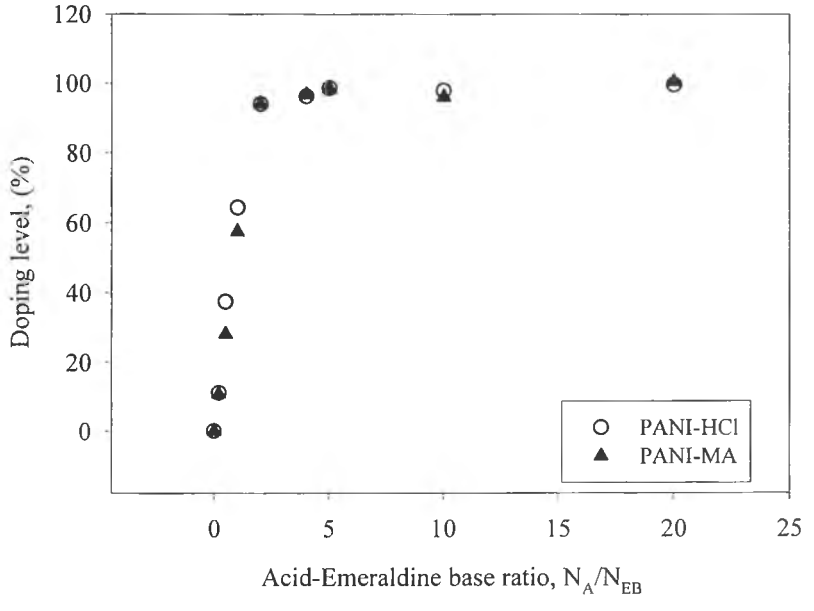

Figure 4.6 Relation between doping level of PANI-HCl and PANI-MA powder and acid-emeraldine base mole ratio.

4.1.2.3 FT-IR measurement

Figure 4.7 shows FT-IR spectra of PANI-HCl at various doping ratios. After doping PANI with HCl, the intensity values of 1498 cm^{-1} and 1590 cm^{-1} peaks increased with increasing dopant concentration. Moreover, the intensity of the main absorption peak at 1160 cm^{-1} increased relative to that of the peak at 1498 cm^{-1}. In earlier study, the peak at 1590cm^{-1} was identified with the quinoid ring stretching and the one at 1498 cm^{-1} was associated mainly with the benzenoid ring stretching of polyaniline (Salaneck, 1993). PANI-HCl spectra indicate that a large portion of the quinoid structure unit in PANI molecular chains was converted to benzeniod structure units, hence, the PANI-HCl spectra support a structure rich in benzeniod units which increased in their amount as doping level increased. In addition, the 1160 cm^{-1} peak is considered as a characteristic peak for

the electron delocalization in polyaniline, which increased with increasing doping level.

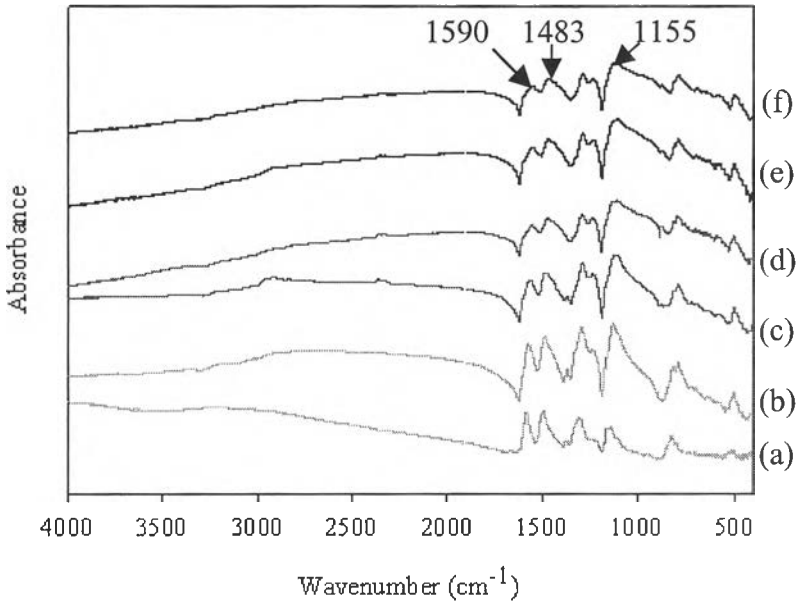

Figure 4.7 FT-IR spectra of PANI-HCl at various doping ratios: (a) EB, (b) N_A/N_{EB} = 0.5, (c) N_A/N_{EB} = 1.0, (d) N_A/N_{EB} = 2.0, (e) N_A/N_{EB} = 10.0 and (f) N_A/N_{EB} = 20.0.

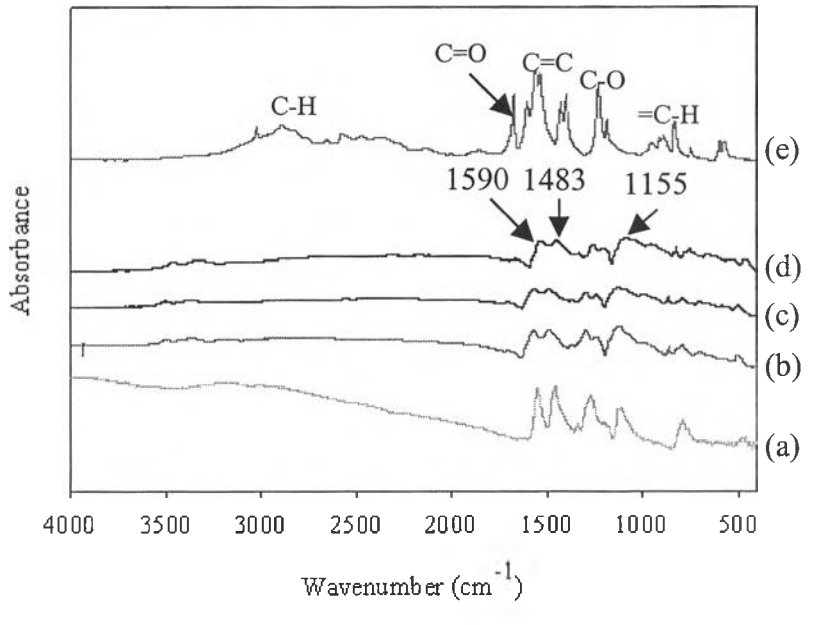

Figure 4.8 FT-IR spectra of PANI-MA at various doping ratios: (a) EB, (b) N_A/N_{EB} = 1.0, (c) N_A/N_{EB} = 2.0, (d) N_A/N_{EB} = 10.0, (e) maleic acid.

The PANI-MA spectra in Figure 4.8 could not be observed clearly because the absorption bands due to the stretching of C=C group of maleic acid at 1480-1600 cm^{-1} affected the stretching vibration bands of N-quinoid ring (1590 cm^{-1}) and N-benzenoid ring (1498 cm^{-1}) of PANI-MA. The FT-IR peaks of emeraldine base and acid-doped polyaniline are summarized in Table 4.4.

Table 4.4 Summarized FT-IR peaks of emeraldine base and acid-doped polyaniline

Functional group	Wavenumber (cm-1)				References
	Undoped	PANI-HCl	PANI-MA	MA	
C-H stretching of acid	-	-	-	3000 [2959]	The Aldrich library of FT-IR Spectra
Stretching of C=O group of acid	-	-	1705	1705 [1707]	
Stretching of C=C group of acid	-	-	-	1480, 1680 [1461, 1591]	
Stretching vibration of N-quinoid ring	1590 [1586]	1593 [1564]	1556	-	Zeng and Ko, (1998)
Stretching vibration of N-benzenoid ring	1483 [1493]	1493 [1484]	1496	-	Zeng and Ko, (1998)
Stretching of C-O group of acid	-	-	-	1308 [1267]	The Aldrich library of FT-IR Spectra
Stretching vibration of C-N	1302 [1297]	1302 [1298]	1303	-	Zeng and Ko, (1998)
Vibration mode of quinoid ring	1155 [1161]	1155 [1150]	1223	-	Zeng and Ko, (1998)
=C-H out of plane bending	-	-	-	675-1000 [874]	The Aldrich library of FT-IR Spectra
C-H bending vibration of para-couple benzene ring	824 [825]	824 [804]	866	-	Zeng and Ko, (1998)

According to the Beer's law (Chambell and White, 1989)

$$A_i = a_i b_i c_i \qquad (B.1)$$

where A_i = area of each peak

a_i = absorptivity (cm^2/g)

b_i = path length (cm)

c_i = concentration of emeraldine base in solution (g/cm^3)

The increase in the doping level of PANI-HCl with the dopant concentration was confirmed by the FT-IR results. To obtain the doping level of PANI-HCl, the amounts of the benzenoid (C=C) to quinoid part (-N=) in a sample were determined by converting the absorbency of each peak to concentration as shown in Appendix B. The percentage of doping level of PANI-HCl is shown in Table 4.5. Figure 4.9 shows the relation between the percentage of doping level of PANI-HCl powder and acid-emeraldine base mole ratio by FT-IR measurement.

Table 4.5 Percentage of doping level of PANI-HCl by FT-IR technique

N_A/N_{EB}	%Doping level
0.0	21.77
0.2	23.03
0.5	43.75, 37.26
1.0	61.30, 43.20
2.0	82.27, 79.27
4.0	87.66
5.0	107.61, 89.80
10.0	93.01, 95.70
20.0	113.88

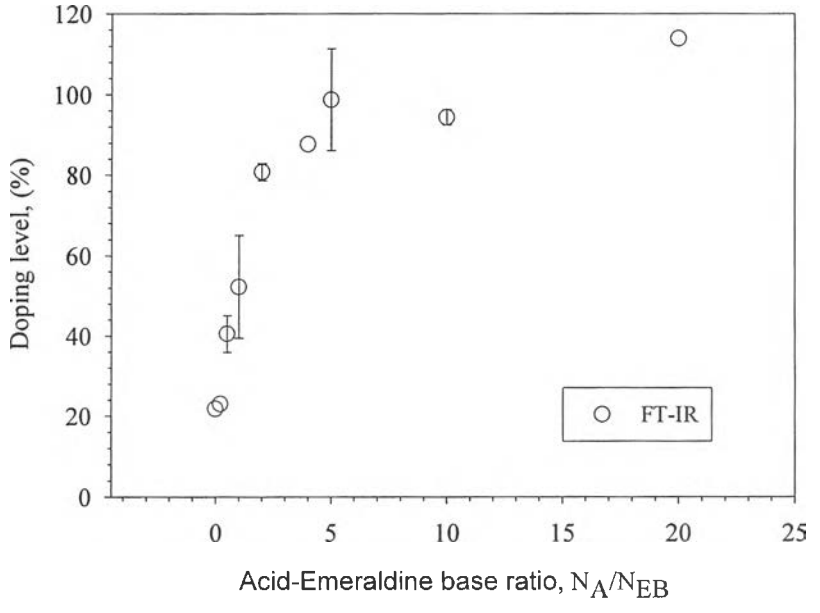

Figure 4.9 Relation between doping level of PANI-HCl powder and acid-emeraldine base mole ratio by FT-IR measurement.

4.1.2.4 UV-vis measurment

Figure 4.10 shows the adsorption spectra of PANI-HCl in NMP solution at different dopant concentrations between the wavelengths of 300-900 nm. It could be seen that the two absorption peaks representing EB could still be observed at acid-emeraldine base ratio $N_A/N_{EB} < 2$. This indicates that there was no change in the molecular structure at lower acid concentrations. As N_A/N_{EB} increases above 2, new absorption peaks at 450 nm and 900 nm were observed whereas the absorption at 633 nm representing the quiniod segments disappeared completely. The new absorption peaks at 450 nm and 910 nm can be identified as the bipolaron and polaron states, respectively. This result clearly confirms that protons of HCl induced the protonation of the imine nitrogen (=N-) on the segment to create the new chemical structure.

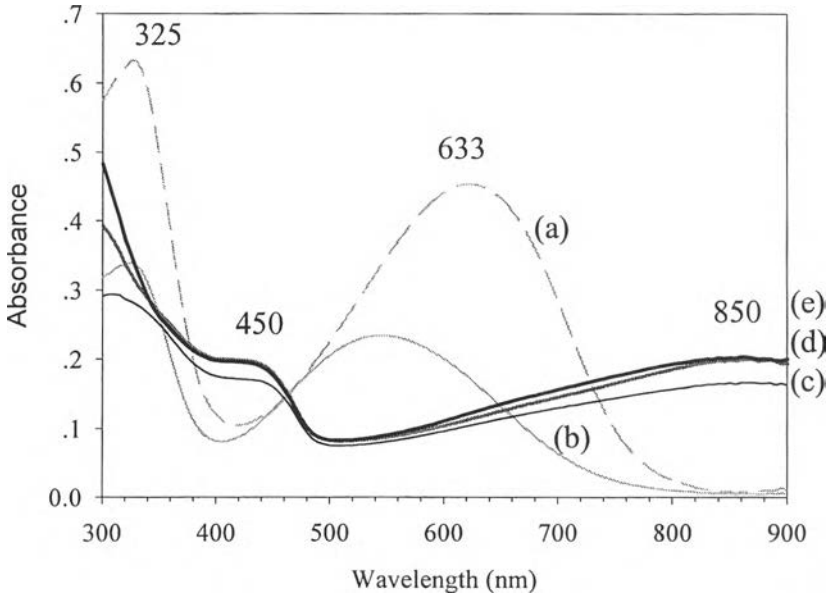

Figure 4.10 UV-visible spectra of PANI-HCl solution in NMP at various doping ratios: (a) EB, (b) N_A/N_{EB} = 1.0, (c) N_A/N_{EB} = 2.0, (d) N_A/N_{EB} = 10.0, (e) N_A/N_{EB} = 20.0.

Figure 4.11 shows the UV-vis spectra of PANI-MA solutions at various dopant concentrations. It could be observed that the PAMI-MA spectra at N_A/N_{EB} between 0-20 show the same absorption peaks as those of EB. This result suggests that the concentration of MA was not sufficient to convert an EB to ES. The EA result shows that the doping level of PANI-MA is close to PANI-HCl; this suggests that NMP, a basic solvent, in the sample preparation neutralized MA is a weak acid. So the structure of PANI-MA could not be observed. The NMP solvent can affect the absorption of PANI-HCl as MacDiarmid *et al.* (1985) reported that the absorption of polaron at 900 nm was only observed for fully protonated PANI whereas the absorption at 630 nm completely disappeared, except for absorption band at 325 nm.

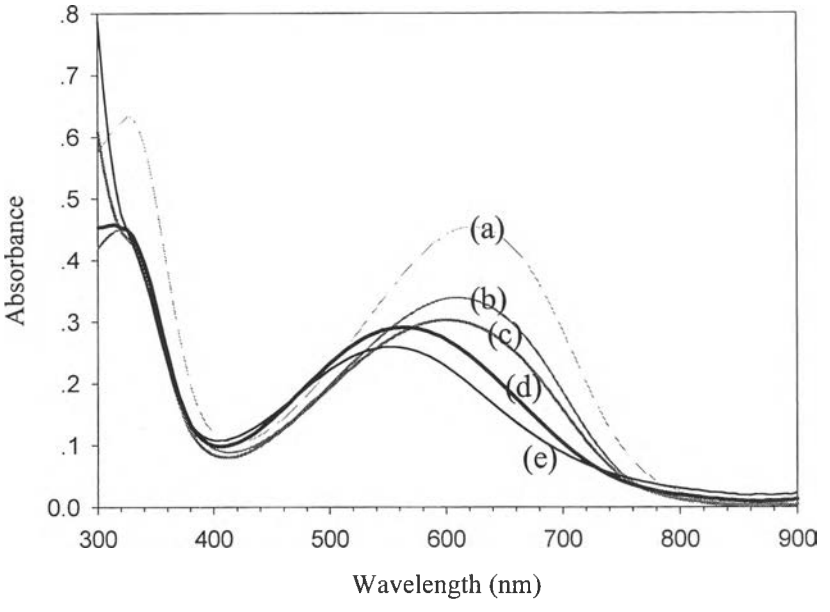

Figure 4.11 UV-visible spectra of PANI-MA solution in NMP at various doping ratios: (a) EB, (b) N_A/N_{EB} = 1.0, (c) N_A/N_{EB} = 2.0, (d) N_A/N_{EB} = 10.0, (e) N_A/N_{EB} = 20.0.

4.1.2.5 XRD measurement

Figures 4.12-4.13 show the diffraction patterns of emeraldine base and all acid-doped polyanilines. Emeraldine base was typically of an amorphous polymer. It probably had a compact coil structure resulting from the H-bonding between amine and imine positions. When polyaniline was protonated by HCl and MA dopants, the protonation at imine nitrogen occurred producing positive charges along the chain. Due to the repulsive forces between the positive charges along the chain, an expansion of the polyaniline coils structure occurred and could be observed. As a result, PANI-HCl and PANI-MA were semicrystalline polymers.

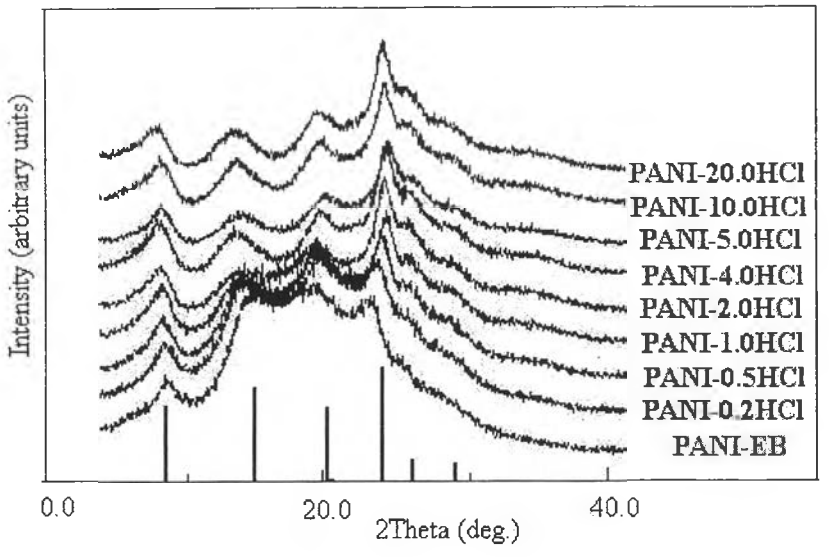

Figure 4.12 XRD patterns of polyaniline emeraldine base and PANI-HCl in pellet form at various doping ratios.

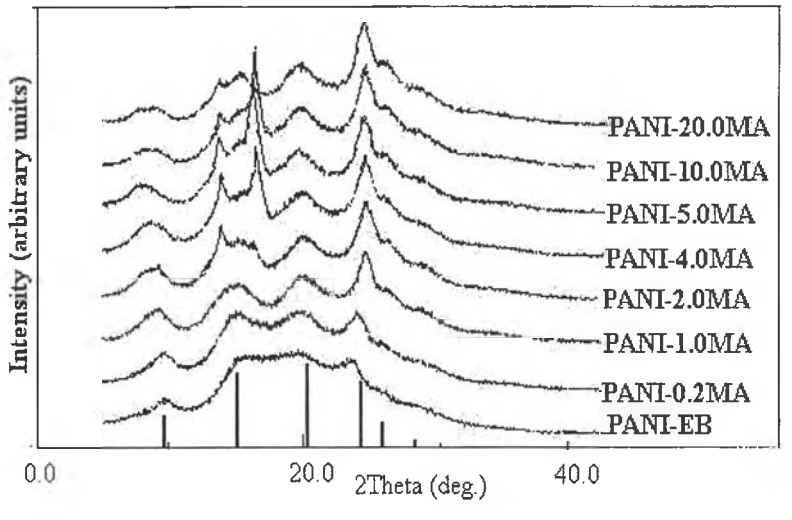

Figure 4.13 XRD patterns of polyaniline emeraldine base and PANI-MA in pellet form at various doping ratios.

Pouget *et al.* (1991) proposed that polyaniline is a pseudo-orthorombic unit cell. The effect of crystallinity structure can be a consequence of the insertion of anions between polymer chains. This adds the Coulomb force between polymer chains

making the structure more rigid and favoring the crystalline state. Anion is positioned in the plane of the nitrogen atom as shown in Scheme 4.1.

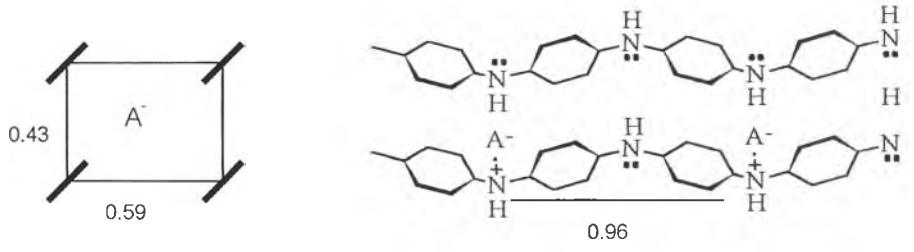

Scheme 4.1 Pseudo-orthorombic unit cell of acid doped polyaniline

Two components of the diffraction intensity can be identified: the crystalline one corresponds to a relative sharp peak, and the amorphous one is visible as a broad band (Lunzy and Banka, 2000). The amorphous component, including the background and the crystalline components were fitted by the sum of an appropriate number of Gaussians. Quantitatively, the percentage of crystallinity was calculated from the ratio of the integrated crystalline component intensity to the integrated total intensity as shown in Appendix C. The degrees of crystallinity of PANI-HCl and PANI-MA are reported in Table 4.6. Figure 4.14 indicates that the degree of crystallinity of polyaniline initially increases with the doping level and then remains constant for higher doping levels.

Table 4.6 Crystallinity and doping levelof PANI-HCl and PANI-MA

N_A/N_{EB}	PANI-HCl		PANI-MA	
	%Doping level	%Crystallinity	%Doping level	%Crystallinity
0.2	11.06	30.9	10.76	30.9
0.5	37.48	34.4	28.1	35
1.0	64.42	44.9, 47.2	57.48	45.8, 41.2
2.0	94.02	54.8, 57.2	94.16	45.2, 43.2
4.0	96.34	57, 53.3	96.74	46.2, 47.8
5.0	98.66	56.0	98.58	51.7
10.0	97.9	53.1, 55.1	96.08	54.5, 57.7
20	99.56	57.5, 51.8	100.46	51.0, 61.4

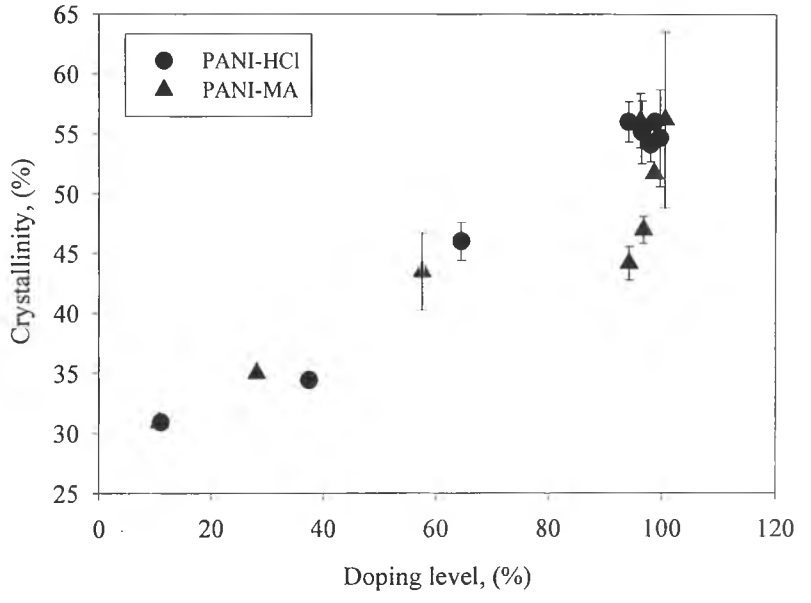

Figure 4.14 Relation between crystallinity and doping level.

4.1.2.6 Scanning electron microscope (SEM)

The undoped and acid-doped polyaniline powders were examined by SEM in order to identify and to understand the relations between microstructures and electrical properties. From Figures 4.15 to 4.16, the morphology of undoped polyaniline is similar to those of PANI-HCl and PANI-MA, which generally has a globular structure.

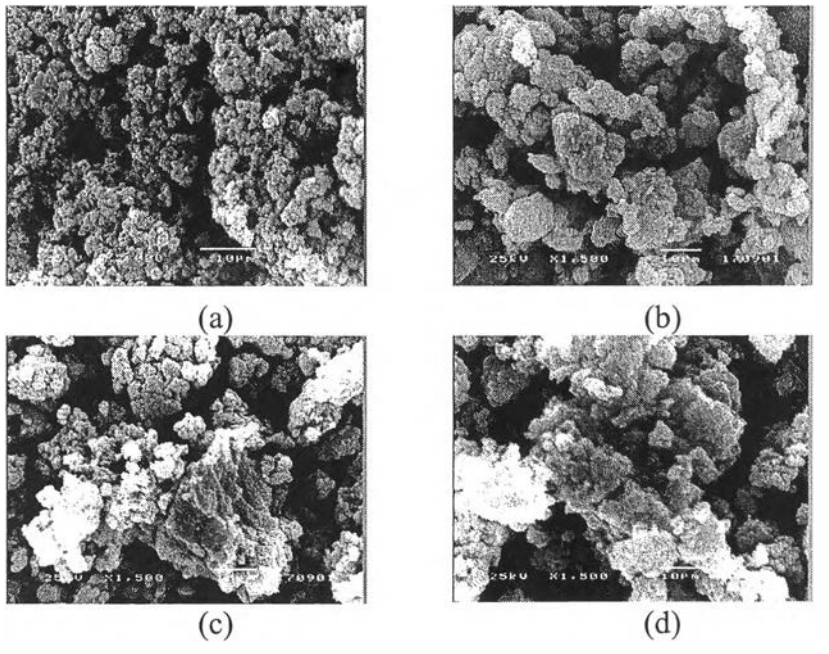

Figure 4.15 Morphological structure of PANI-HCl at various doping ratios: (a) PANI-EB, (b) N_A/N_{EB} = 1.0, (c) N_A/N_{EB} = 10.0, and (d) N_A/N_{EB} = 20.0.

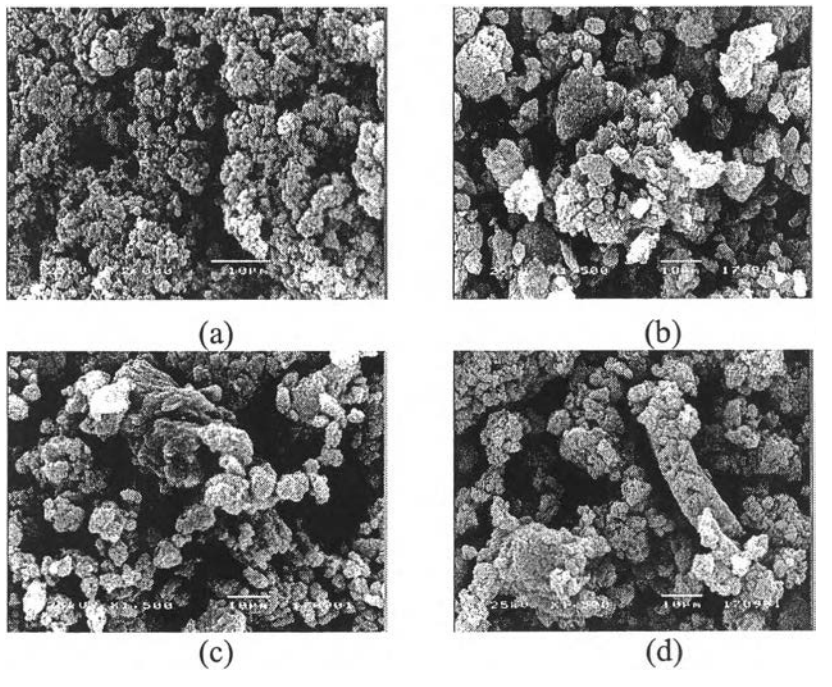

Figure 4.16 Morphological structure of PANI-MA at various doping ratios: (a) PANI-EB, (b) N_A/N_{EB} = 1.0, (c) N_A/N_{EB} = 10.0, and (d) N_A/N_{EB} = 20.0.

For PANI-HCl and PANI-MA at a doping ratio < 20.0, a globular structure can be observed because the repulsive forces between positive charges along the chain were smaller than that of the forming of intramolecular hydrogen bonding between amine and imine positions. However, the structures PANI-MA observed at the doping ratio of 20.0 seem to be fibrillar. Sangswarng (2001) reported that a fibrillar structure of PANI-MA could be seen at doping ratios of more than 40 due to the repulsive forces between positive charges along the chain and the intermolecular hydrogen bonding. It was interesting to observe that upon increasing the doping ratio, the morphology of the conductive polymer changed from having typical three-dimensional random coil, granular structure to rigid rod-like, fibrillar structures (Sangswarng, 2001).

4.1.3 Conductivity of Acid-Doped Polyaniline

Figure 4.17 shows the relation between the specific conductivity and the %doping level of PANI-HCl and PANI-MA at 26-28°C, relative humidity 60±5° C at the atmospheric pressure. The electrical conductivity of PANI-HCl and PANI-MA slightly increased with the increase of the doping level. The electrical conductivity of PANI-HCl reached equilibrium value of about 4 S/cm at saturated doping level. In comparison with PANI-MA, the electrical conductivity reached its equilibrium value of about 5 S/cm. This indicates that the electrical conductivity increase is directly due to the increase of the doping level but it was independent of the effect of dopant type.

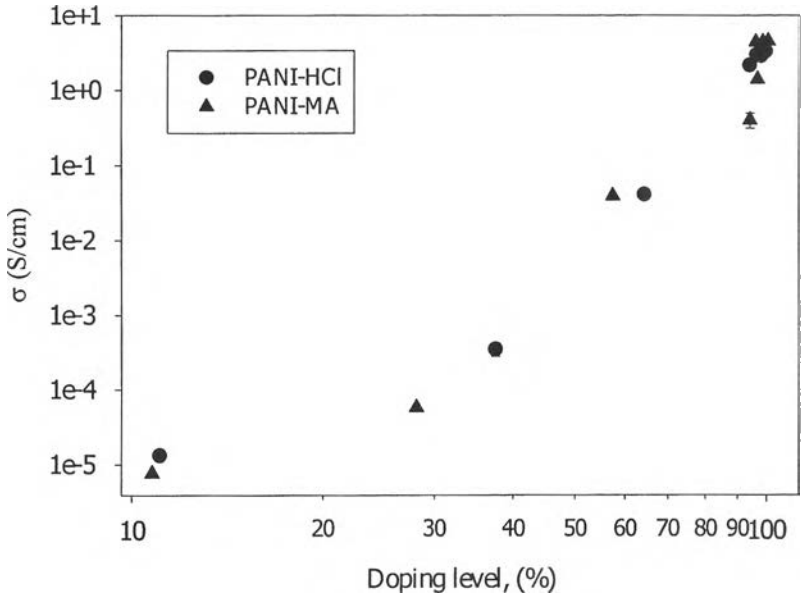

Figure 4.17 Effect of the doping level on the specific conductivity as determined by EA technique.

This can be explained by a conductivity theory (Cowie, 1991). The conductivity (σ) is a function of the charge carrier (e), number of charge carrier per unit volume (n) and charge mobility (μ) according to Equation 1.1.

$$\sigma = ne\mu \tag{1.1}$$

The increase of doping level is proportional to the increase in the number of charge carrier. However, the relation between electrical conductivity and doping level is nonlinear as shown in Figure 4.17 because the electrical conductivity of conductive polymer could be also affected by the molecular structure. Next, the effect of crystalline structure on specific conductivity was studied. From the conductivity theory, Figure 4.18 shows the correlation between σ/n and %crystallinity. The electrical conductivity divided by %doping level, (σ/n), should be proportional to the charge mobility (μ). We can see that σ/n follows a power law function of %crystallinity for both PANI-HCl and PANI-MA as:

$$\sigma/\%\text{Doping level} = a\,[\%\text{Crystallinity}]^{b} \qquad (4.1)$$

The electrical conductivity can be largely affected by the crystallinity of polymer. For PANI-MA, b = 22 is larger than b of PANI-HCl which was found to be 17. We can conclude that charge mobility is a power law function of %crystallinity. The metallic island model can be used to explain this result.

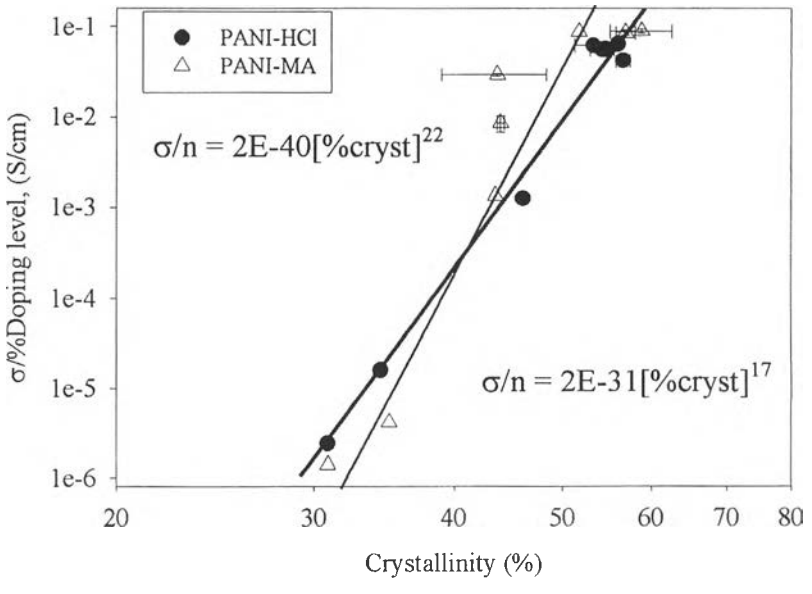

Figure 4.18 Specific conductivity/%doping level as a function of %crystallinity.

In previous studies (Pouget, 1991), They explained that polyaniline can be characterized as an inhomogeneous disorder metal state comprised of metallic islands (ordered) surrounded by insulating barriers (disordered). It is also called the metallic island model as shown in Scheme 4.2 (a). A number of experiments (Kahol *et al.*, 1997) has been performed which led them to propose a 'variable-size metallic island' model as shown in Scheme 4.2 (b). That is, protonated and highly ordered regions (metallic islands) are separated from unprotonated and amorphous regions by a less ordered region, whose width depends on the amount of moisture present in the sample. The water reduces the width of the boundary region by introducing order and thereby transforming partly localized polarons into either delocalized polaron or

was proposed that the conductivity enhancement is due to increased size of the metallic islands in the presence of moisture.

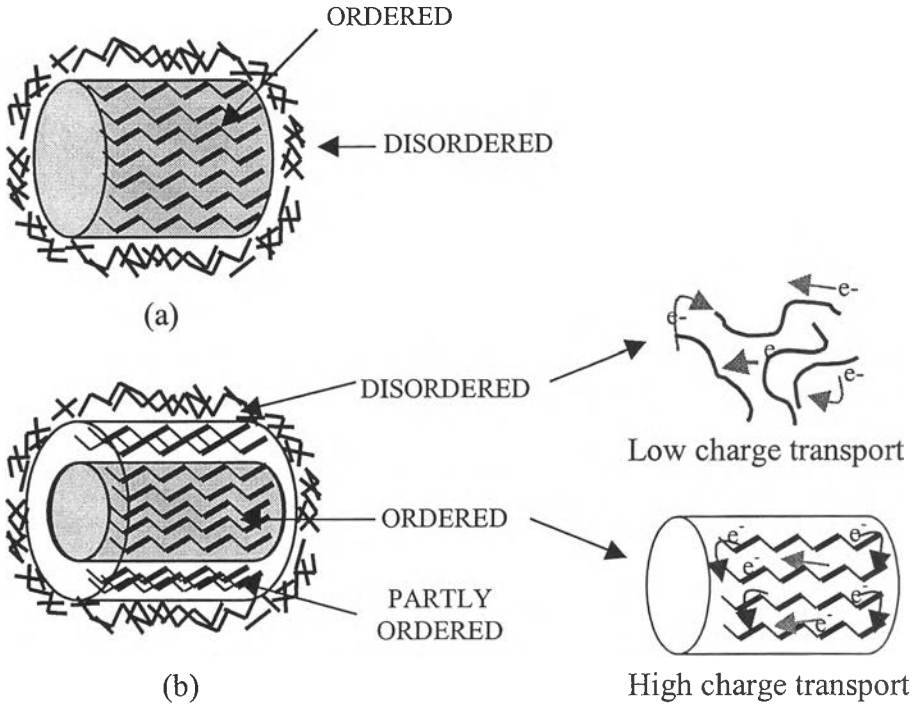

Scheme 4.2 Schematic representation of the inhomogeneous metallic island' model (a) the variable–size metallic island modal (b). In the two latter models, ordered regions are separated from disordered region by a region comprised of partly ordered chains

For the effect of doping level, the increase of doping level can induce significant differences in crystallinity structure, which means that metallic islands of different sizes exist in the disordered regions. A metallic island of a smaller size the lower electrical conductivity and only a quasi-one dimensional charge transport behavior, whereas a more highly ordered island exhibits an enhanced conductivity and an increase in charge transport along the chain and interchain coupling as shown in Scheme 4.2 (b).

4.1.4 Sensitivity and Interaction of Acid-Doped Polyaniline to CO

HCl-doped polyaniline (PANI-HCl) and MA-doped polyaniline (PANI-MA) pellets of different dopant types, doping levels and crystallinity were exposed to CO at various concentrations in order to investigate the sensitivity and scaling exponent.

4.1.4.1 Carbonmonoxide interaction

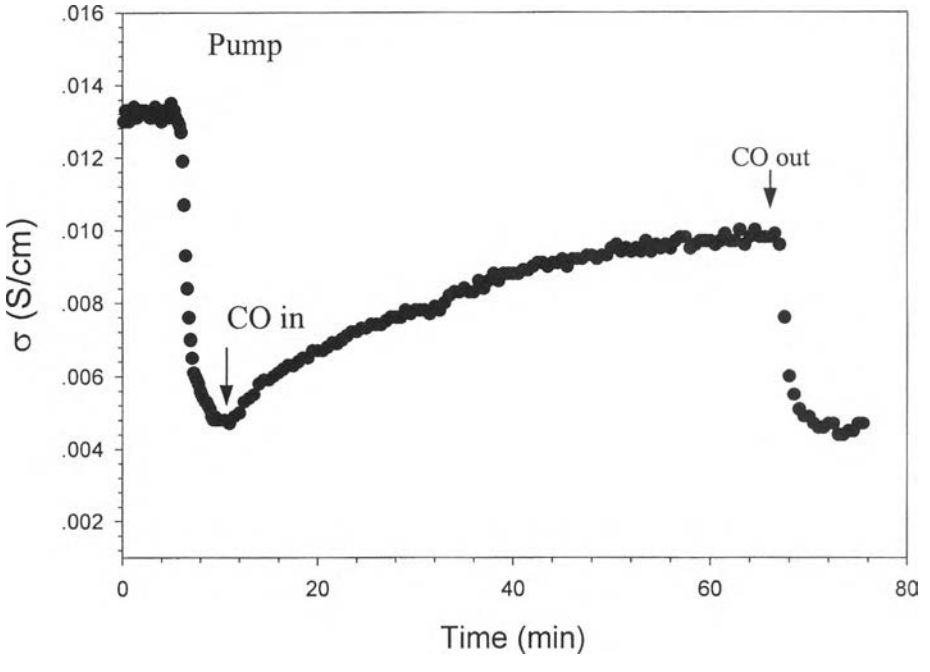

Figure 4.19 Effects of vacuum, and CO on the specific conductivity of PANI-HCl pellet, N_A/N_{EB} = 1.0 at 1 atm, 27-28°C, and 65-69% relative humidity.

Figure 4.19 shows that the effects of vacuum, and carbon monoxide (CO) on the specific conductivity of PANI-HCl pellet, N_A/N_{EB} = 1.0 at 27-28°C and 65-69% relative humidity. Using a vacuum pump led to a decrease in conductivity by an order of magnitude and it became constant after approximately 10 min due to the water desorption (Kohol, 1997 and Kang, 1999). The effect of water on the specific conductivity of polyaniline has been well documented (Kahol, 1997). The effect of CO on the acid doped polyaniline shows that an exposure to CO gas

produced an increase in conductivity, its value continued to rise and became constant. After the gas was removed and the pellet was under vacuum, the specific conductivity decreased and returned to the original value. The sensitivity ($\Delta\sigma$) can be defined in term of the change of the specific conductivity in nitrogen state to the value in the CO state, σ_{CO}-σ_{N2}. The period between the injection of CO gas and the time when the conductivity became constant is called the response time, Δt.

The interaction between CO and the conductive polyaniline can be explained by the mechanism proposed in Scheme 4.3. CO is an electrophillic gas that withdrew an electron lone pair at amine nitrogen on the backbone of polyaniline. When this occurred, the polyaniline became more positively charged. The more positively charges created gave rise to the increase in conductivity of the polyaniline. This is analogous to the well-known increase in conductivity upon protonation for an emeraldine base. This result suggests that acid-doped polyaniline with a higher amine nitrogen should have a higher sensitivity ($\Delta\sigma$).

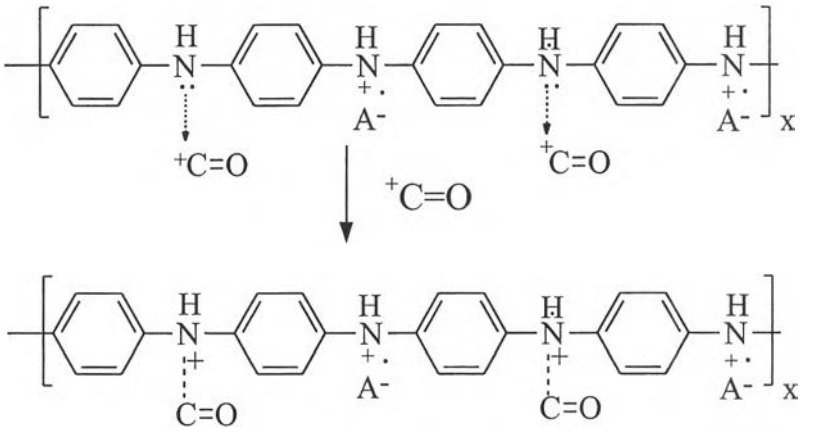

Scheme 4.3 Interaction between CO and the conductive polyaniline

4.1.4.2 Characterization of acid-doped polyaniline upon exposure to CO

4.1.4.2.1 In-situ FT-IR measurement

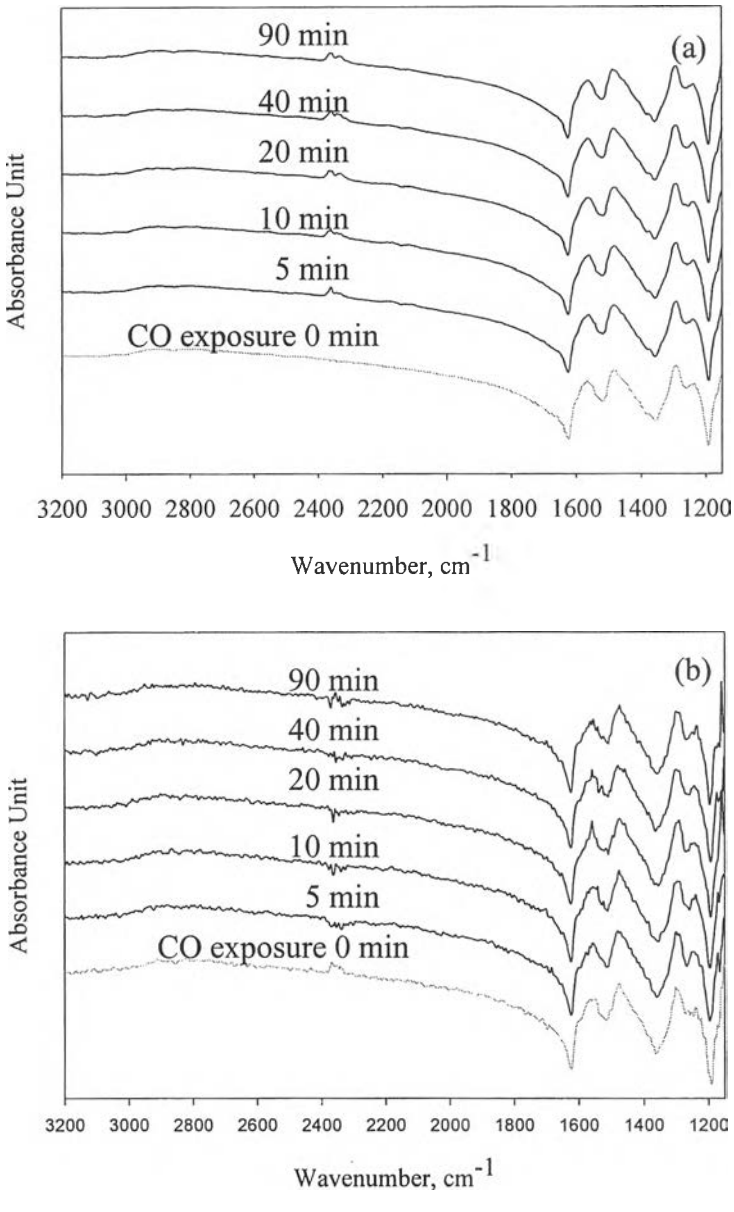

Figure 4.20 FT-IR spectra of PANI-HCl before and in-situ exposure to 1000 ppm CO/N_2 mixture: (a) PANI-1HCl and (b) PANI-10HCl.

Figure 4.20 shows FT-IR spectra of PANI-1HCl and PANI-10HCl before and in-situ exposure to 1000 ppm CO/N_2. There is no difference

in the FT-IR spectra before and in-situ exposure to CO. This indicates that CO did not chemically interact with the polyaniline. CO molecules only physically adsorbed onto the polyaniline chain and desorption of CO molecules occurred after a vacuum process.

4.1.4.2.2 XRD measurement

XRD technique was used to investigate the difference in crystalline structure of acid doped polyaniline after exposed to 1000 CO more than 3 days. Figure 4.21-4.22 shows the XRD pattern of PANI-HCl and PANI-MA before and after exposed to CO, respectively. From Figure 4.21 to 4.22, there is no difference in the XRD pattern before and after exposed to CO. This indicates that the crystallinity of acid doped polyaniline did not change after exposed to CO but this result could not be conclued clearly. Because the crystallinity of polyaniline may be changed during the CO exposure but it was reversible after the gas was removed by vacuum. By the limitation of instrument, further work is required to confirm the effect of cyrstallinity on the CO exposure by taking in-situ XRD measurement. This was because of the crystalline structure is largely affected to the electrical conductivity and sensitivity of acid doped polyaniline.

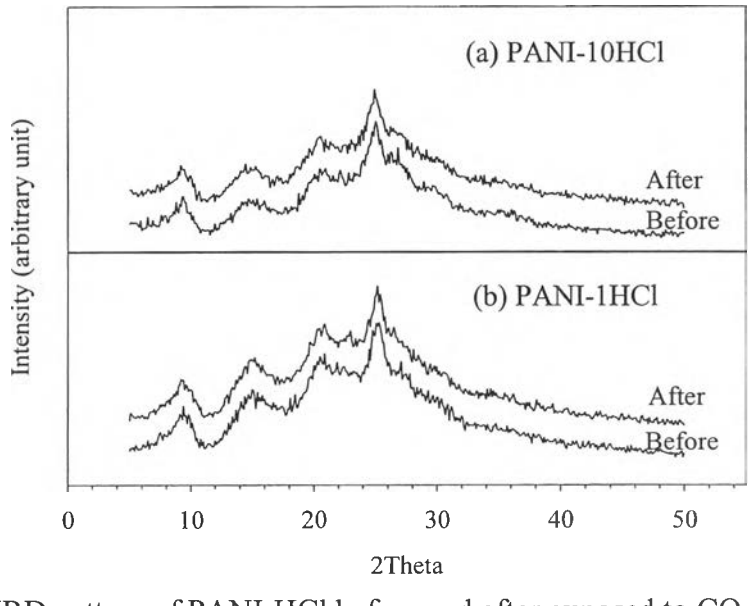

Figure 4.21 XRD pattern of PANI-HCl before and after exposed to CO.

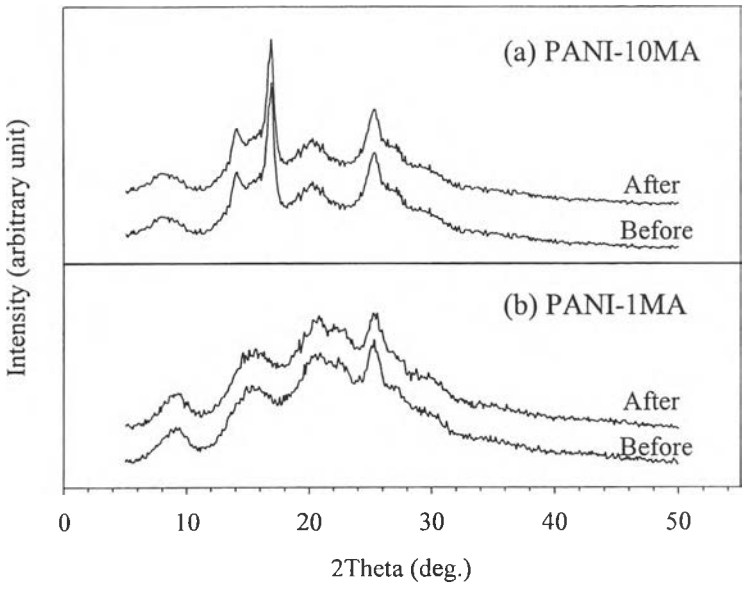

Figure 4.22 XRD pattern of PANI-MA before and after exposed to CO.

4.1.4.3 CO sensitivity of acid doped polyaniline

Figures 4.23 shows the relation between the change in the electrical conductivity or sensitivity ($\Delta\sigma$) and CO concentration of HCl-doped polyaniline at N_A/N_{EB} = 1.0, (PANI-1HCl) and N_A/N_{EB} = 10.0, (PANI-10HCl) in which each CO concentration was allowed a fixed exposure time of approximately 60-min. This graph shows that $\Delta\sigma$ of PANI-1HCl is higher than PANI-10HCl when exposed to CO at various concentrations. This was because the %doping level of PANI-1HCl was lower than PANI-10HCl as shown in Table 4.8. The %doping level indicates the number of active site on polymer chain that interacted with CO molecule. When the interaction occurred, the polyaniline became more positively charged. The increase of positively charges (Δn) created gave rise to the increase in conductivity ($\Delta\sigma$). This means that the lower doping level gave the higher increment of charge carrier (Δn). This result suggests that PANI-HCl, which has a low doping level, should be have a high sensitivity. So, we can conclude that CO sensitivity of HCl-doped polyaniline could be affected by the %doping level.

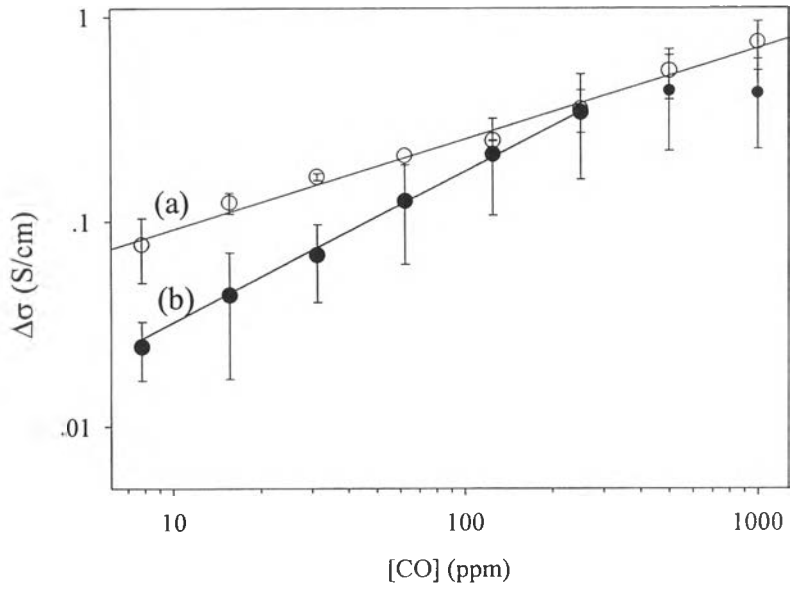

Figure 4.23 Relation between Δσ and [CO] of PANI-HCl at 1 atm, 27-28°C and 65-69% relative humidity; (a) N_A/N_{EB} = 1.0 and (b) N_A/N_{EB} = 10.0.

Table 4.7 Characteristic of acid doped polyaniline pellet

Dopant	N_A/N_{EB}	%Doping level	%Crystallinity	b
HCl	1	32	46	17
	10	49	54	
MA	1	29	43	22
	10	48	56	

* $\Delta\sigma = a[CO]^b$, b = Slope of curve

Figures 4.24 shows relation between Δσ and CO concentration of maleic acid-doped polyaniline at N_A/N_{EB} = 1.0, (PANI-1MA) and N_A/N_{EB} = 10.0, (PANI-10MA). This graph shows that the sensitivity of PANI-1MA is much lower than PANI-10MA that while the number of active site of PANI-1MA had higher than PANI-10MA. This result contrasted with the result of PANI-HCl as shown in Figure 4.23.

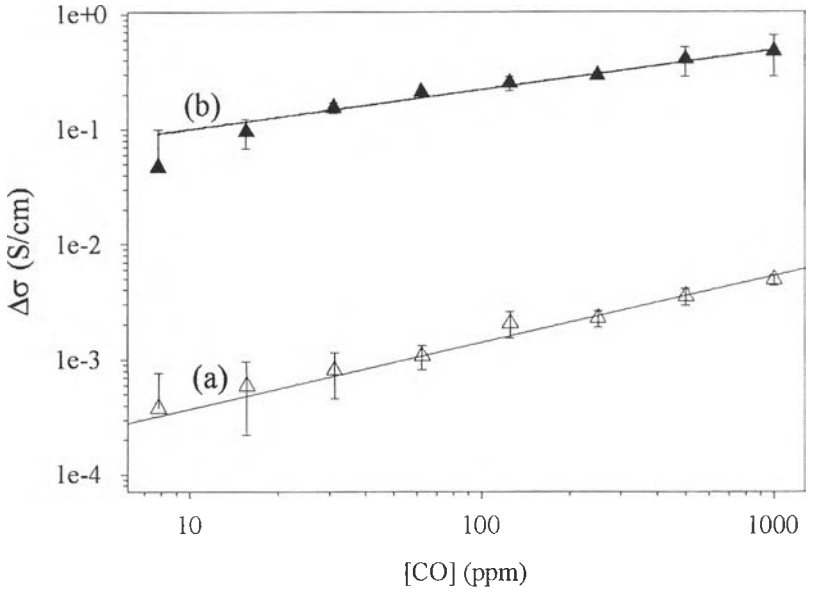

Figure 4.24 Relation between $\Delta\sigma$ and [CO] of PANI-MA at 1 atm, 27-28°C and 65-69% relative humidity; (a) N_A/N_{EB} = 1.0 and (b) N_A/N_{EB} = 10.0.

This was because the effect of different dopant types between MA and HCl. This effect can be supported by the largely different sensitivity of PANI-1HCl and PANI-1MA at the same percentage of doping level. The data indicates that the interaction between CO and active site of PANI-MA was more difficult than of PANI-HCl. It should be the obstruction of MA anion that has a larger size than Cl anion. From the effect of dopant, the sensitivity of PANI-MA was less affected by the doping level than PANI-HCl.

In comparison between PANI-10MA (Figure 4.24) and PANI-10HCl (Figure 4.23), which have the same %doping level and crystalliniliy structure as listed in Table 4.7, the data show that the sensitivity of PANI-10MA became close the sensitivity of PANI-10HCl. This result suggests that some of sensitivity enhancement may be associated with the charge mobility (μ) in term of the change of the morphology from having granular structure to rigid rod like to a fibrillar structure when exposed to CO. The other factor should be the increase of crystallinity structure upon exposure to CO. In previous studies (Pouget, 1991), the change of

and crystallinity of acid-doped polyaniline is largely affected the charge mobility of conductive polyaniline. So the conductivity increment of PANI-10MA could be function to the increase of charge mobility on the polymer chain. For the increase in the number of charge mobility ($\Delta\mu$) we had no evidence because of the limitation of instrument. So, the sensitivity or conductivity increment of acid-doped polyaniline upon exposure to CO depended on two types of effects. They are (i) the increase in the number of charge carrier (Δn) and (ii) the increase of charge mobility ($\Delta\mu$) on the polymer chain according to Equation 4.2 that is derived from Equation 1.1: $\sigma = en\mu$.

$$\Delta\sigma = e(\mu\Delta n + n\Delta\mu) \tag{4.2}$$

The increase in the number of charge carrier (Δn) can be explained by the effect of doping level whereas the increase in the number of charge mobility ($\Delta\mu$) can be explained by the effect of morphology and crystallinity structure. Both Figures 4.23 and 4.24 show the conductivity increment of all samples increased with CO concentration according to a power law equation:

$$\Delta\sigma = a[CO]^b \tag{4.3}$$

where b is a scaling exponent characterizing concentration dependence and a is the scaling prefactor. The minimum threshold concentration level was at least 8 ppm for all samples. The maximum threshold concentration level was at least 1000 ppm for PANI-1HCl, PANI-1MA and PANI-10MA but that was about 250 ppm for PANI-10HCl. The scaling exponent, scaling prefactor and conductivity of each sample are listed in Table 4.8

Table 4.8 Scaling exponent, scaling prefactor, and conductivity of all acid doped polyanilines

Dopant	N_A/N_{EB}	σ (S/cm)	a (S/cm)	b
HCl	1	0.04 ± 0.005	$2.47x10^{-2}$	0.43
	10	4 ± 0.3	$5.86x10^{-3}$	0.74
MA	1	0.04 ± 0.005	$1.50x10^{-2}$	0.51
	10	4 ± 0.3	$4.52x10^{-2}$	0.34

The result of b and sensitivity of all samples shows that, PANI-10MA is the most suitable to be used as a CO sensor because it had higher conductivity and sensitivity. Moreover, it can be used in a wider range of gas concentration relative to PANI-10HCl, which had the comparable conductivity and sensitivity.

4.2 Polyaniline/Zeolite Composite

4.2.1 Zeolite Characterization

All types of zeolite A used to form the composite pellet were obtained from Aldrich Chemical CO. They were characterized by using EDS, TGA and particle analyzer measurement

4.2.1.1 Pore size diameter

The zeolite A is normally synthesized in the Na^+ form. Typical unit cell content of zeolite A = $Na_{12}Al_{12}Si_{12}O_{48}27H_2O$ with a pore diameter ~4Å referred to zeolite 4A. The different window size of the zeolite type A is due to the cation present. The EDS results show that zeolite 3A had K^+ and Na^+ ions present in the pore structure, whereas zeolite 5A had Ca^{2+} and Na^+ as listed in Table 4.9. For zeolite 3A, Na^+ is replaced with a larger K^+ ion in a similar position, the window size is reduced to 3Å. For zeolite 5A, Ca^{2+} ions are exchanged for $2Na^+$ ions, this process produces the window size as large as 5Å.

Table 4.9 Window size diameter of zeolite A powder at different cation

Zeolite Name	Typical unit cell content	Pore size diameter(Å)
3A	$K_6 Na_6Al_{12}Si_{12}O_{48}27H_2O$	3
4A	$Na_{13}Al_{13}Si_{13}O_{48}27H_2O$	4
5A	$Ca_2Na_5Al_{11}Si_{11}O_{48}27H_2O$	5

4.2.1.2 TGA measurement

Table 4.10 shows TGA results of all zeolite A samples typically containing the various amounts of adsorbed water ~15-19% at the weight loss between 120-200°C as shown in Figure 4.25. The percentage of water loss gives an indication of the free volume within the zeolite framework. Because of the zeolite framework, channels and voids normally contain cations and water molecules. When the water is removed, a void is created within the framework, which can take in other molecules. For adsorption/diffusion studies, the adsorbed water molecules within the zeolite structure were removed prior to use.

Table 4.10 Weight loss of zeolite A powder at different window sizes

Step loss	Zeolite 3A		Zeolite 4A		Zeolite 5A	
	%loss	Onset (°C)	%loss	Onset (°C)	%loss	Onset (°C)
First-step	2.5 ± 1	61 ± 1	1.7 ± 0.2	57 ± 1	3 ± 0.5	44 ± 2
Second-step	15 ± 1	142 ± 1	15 ± 1	137 ± 1	8 ± 1	120 ± 2
Third-step	-	-	2 ± 1	345 ± 1	8 ± 1	183 ± 1

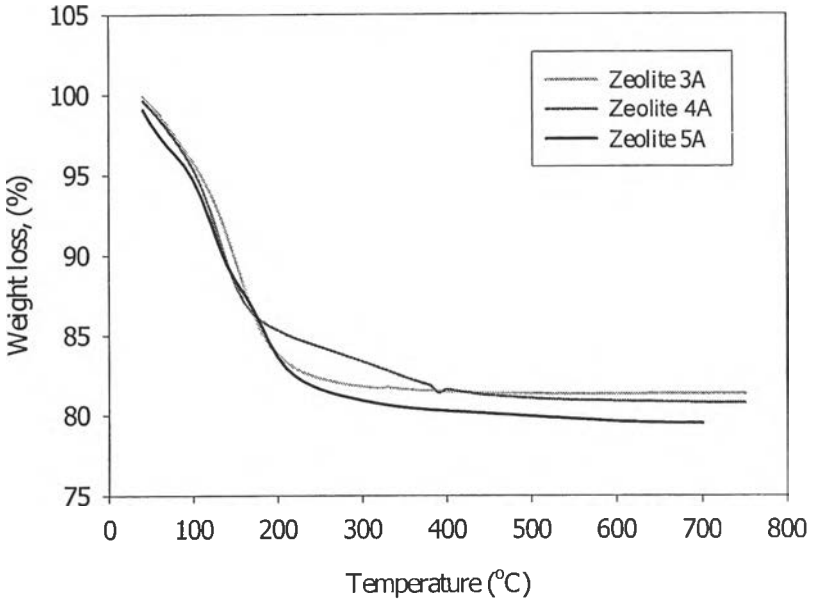

Figure 4.25 Thermogram of zeolite A powder.

4.2.1.3 Particle size analysis

Zeolite 3A had a particle size ~15 μm which is bigger than zeolite 4A and 5A which have diameter sizes between ~4-7 μm, as listed in Table 4.11. The particle size distribution of zeolite 4A is shown in Figure 4.26

Table 4.11 Average particle size of zeolite A powder at different window size diameter

Zeolite Name	Mean Diameters (μm)			Average particle size diameter (μm)
	Sample1	Sample2	Sample3	
3A	15.11	15.35	15.02	15.16
4A	3.64	3.65	3.67	3.59
5A	7.37	7.44	7.27	7.36

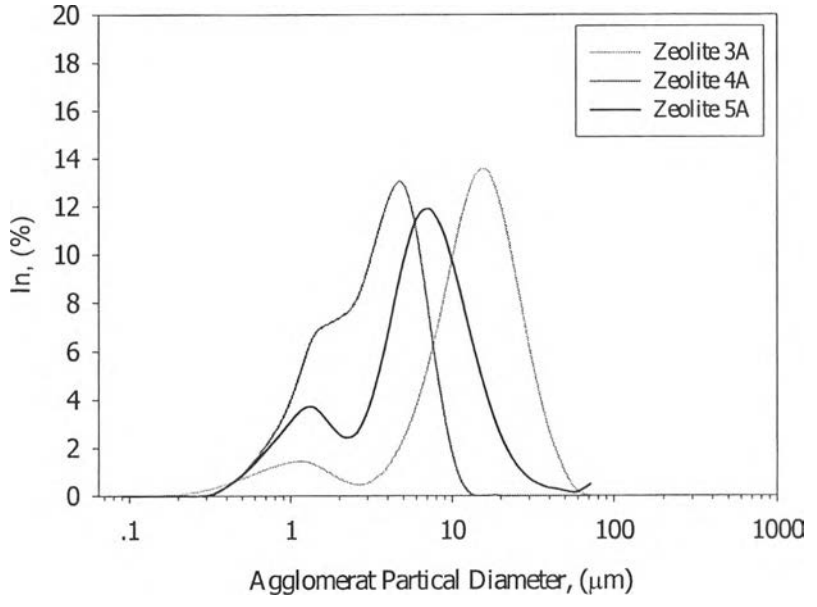

Figure 4.26 Particle size distribution of zeolite A powder.

4.2.2 Polyaniline/Zeolite Composite Characterization

4.2.2.1 Surface distribution of composite sample

Figure 4.27 shows the morphology of zeolite A powders at different window diameters and different particle sizes.

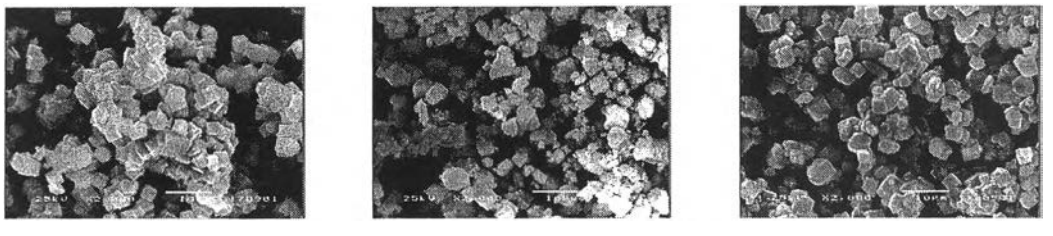

(a) (b) (c)

Figure 4.27 Morphology of zeolite A powders at different molecular structure (x2000): (a) Zeolite NaKA, (3A), (b) Zeolite NaA, (4A), and (c) Zeolite NaCaA, (5A).

An extremely important result of the present study is that upon mixing a zeolite distribution with a polyaniline powder as shown in Figure 4.28, the zeolite powders (white powder) were evenly distributed on the surface of PANI pellets and a homogeneous mixture was obtained.

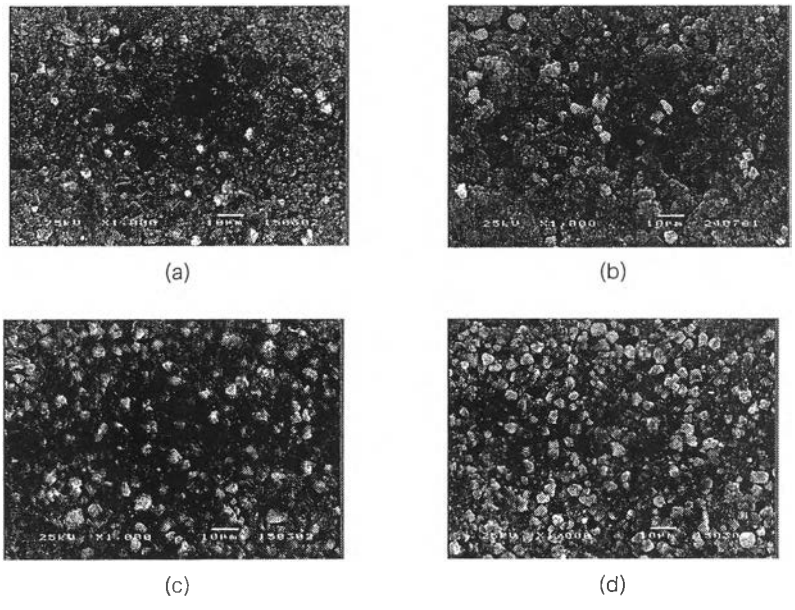

Figure 4.28 Morphology of Polyaniline/Zeolite NaA composite at different zeolite contents (x1000): (a) 5%Zeolite 4A, (b) 10%Zeolite 4A, (c) 30%Zeolite 4A, (d) 50%Zeolite 4A.

4.2.3 Conductivity of PANI/Zeolite 4A Composite

Figure 4.29 shows the electrical conductivity of PANI-10MA/Zeolite 4A composite at various zeolite 4A contents. The electrical conductivity slightly decreased with increasing zeolite content without exhibiting a percolation threshold. The PANI-10MA/50Zeolite 4A had the electrical conductivity of about 0.4 S/cm. The decrease of electrical conductivity of PANI-10MA/Zeolite 4A composite can be thought in terms of the increase of zeolite 4A in free volume within polyaniline matrix.

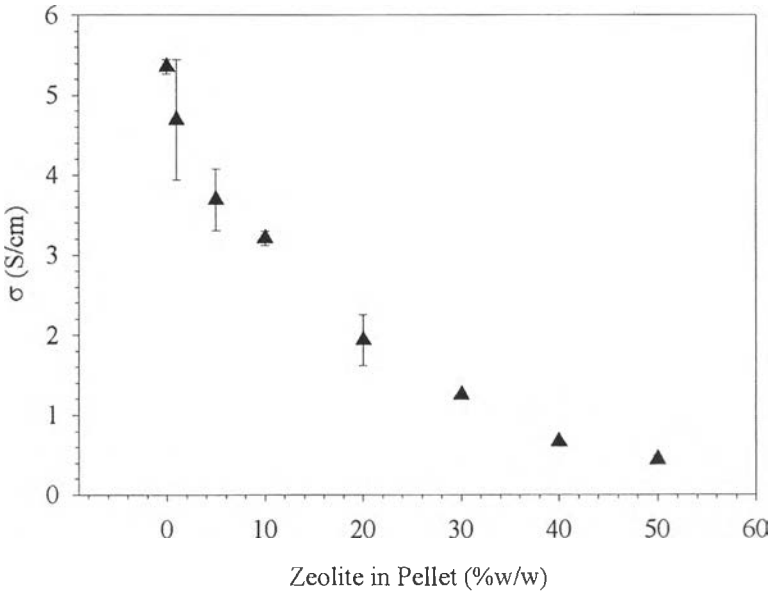

Figure 4.29 Effect of zeolite 4A on specific conductivity of polyaniline pellet.

4.2.4 Sensitivity of PANI-10MA/Zeolite A Composite on CO Exposure

4.2.4.1 Effect of zeolite content on sensitivity

In this work, MA-doped polyanline powder at N_A/N_{EB} = 10, (PANI-10MA), was mixed together with zeolite 4A at various zeolite 4A contents and the resulting pellets were exposed to CO gas in order to investigate the change in the electrical conductivity or sensitivity at various CO concentrations. Figure 4.30 shows the relation between the sensitivity ($\Delta\sigma$) and CO concentration of PANI-10MA/Zeolite 4A composite at different 4A contents. For PANI-10MA/10Zeolite 4A $\Delta\sigma$ was comparable with PANI-10MA sample. For a higher zeolite 4A content (> 20%), $\Delta\sigma$ of PANI-10MA/Zeolite 4A composite decreased with increasing percentage of zeolite 4A content at a particular CO concentration. It was because of the decrease in free volume of PANI-10MA in the composite sample, which decreased the active sites, or amine nitrogens, which can interact with CO molecules.

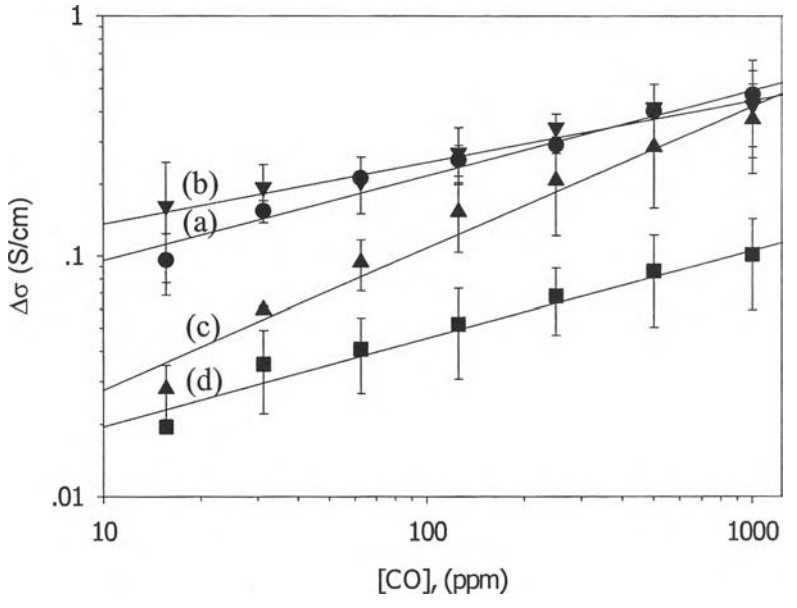

Figure 4.30 Relation between Δσ and CO concentration of PANI-10MA/Zeolite 4A composite in 1 atm, 27-28°C and 65-69% relative humidity; (a) PANI-10MA, (b) PANI-10MA/10Zeolite, (c) PANI-10MA/20Zeolite, and (d) PANI-10MA/40Zeolite in pellet.

In all PANI-10MA/Zeolite 4A composites studied, Δσ increased with increasing CO concentration according to a power law function:

$$\Delta\sigma = a[CO]^b \qquad (4.3)$$

where b is a scaling exponent characterizing concentration dependence. The scaling exponent and scaling prefactor, a, are shown in Table 4.12.

Table 4.12 Scaling exponent and scaling prefactor of PANI-10MA/Zeolite 4A composite

%wt zeolite 4A in PANI pellet	a (S/cm)	b
0	$4.52\text{x}10^{-2}$	0.34
10	$9.50\text{x}10^{-2}$	0.22
20	$1.08\text{x}10^{-2}$	0.52
40	$1.03\text{x}10^{-2}$	0.34

The scaling exponents of all PANI-10MA/Zeolite 4A composite were comparable that of PANI-10MA because it was the common property of PANI-10MA. This confirms that the sensitivity of PANI-10MA/Zeolit 4A composite decreased because of the decrease in the free volume within the PANI-10MA matrix.

4.2.4.2 Effect of zeolite type with different window size diameter on sensitivity

Figure 4.31 shows the relation between sensitivity and CO concentration of PANI-10MA, and PANI-10MA/Zeolite A with different window sizes at a fixed zeolite content. $\Delta\sigma$ of all PANI-10MA/20Zeolite A compolites slightly decreased at a particular CO concentration compared with PANI-10MA sample except for PANI-10MA/Zeolite 4A composite at [CO]<100 ppm. However, all composite samples showed comparable sensitivity values, ($\Delta\sigma$) because they consisted of nearly the same volumes of PANI-10MA.

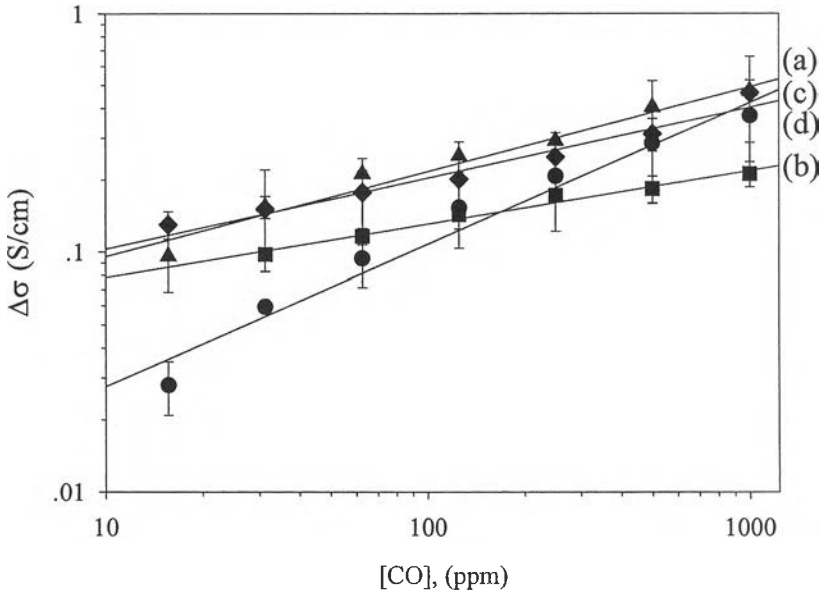

Figure 4.31 Relation between $\Delta\sigma$ and CO concentration of PANI-10MA/Zeolite A composite at 20% zeolite content in 1 atm, 27-28°C and 65-69% relative humidity; (a) PANI-10MA, (b) PANI-10MA/Zeolite 3A, (c) PANI-10MA/Zeolite 4A, and (d) PANI-10MA/Zeolite 5A composite.

In all PANI-10MA/Zeolite A composites studied, $\Delta\sigma$ increased with increasing CO concentration according to a power law equation for PANI-10MA sample:

$$\Delta\sigma = a[CO]^b \quad (4.3)$$

where b is a scaling exponent characterizing concentration dependence. The scaling exponent and scaling prefactor, a, are listed in Table 4.13.

Table 4.13 Scaling exponent and scaling prefactor of PANI-10MA/20Zeolite A composite with different zeolite window size

Zeolite type in PANI pellet	Window size diameter (A°)	a	b
0	-	$4.52\text{x}10^{-2}$	0.34
3A	3	$5.82\text{x}10^{-2}$	0.19
4A	4	$1.08\text{x}10^{-2}$	0.52
5A	5	$4.21\text{x}10^{-2}$	0.34

This result indicates that the zeolite A, which has a window size about 3-5 Å did not affect the sensitivity of PANI-10MA upon exposure to CO. This was because the window size of zeolite A was close to the kinetic diameter of CO about 3.8 Å, it was difficulty for CO molecules to adsorb onto the zeolite structure. Moreover, the operation temperature and pressure on CO exposure may be unsuitable to favor the CO adsorption.

The results suggest that the gas adsorption onto zeolite A structure was a complicated process. Further work is required to study the effect of zeolite on the CO-sensing and the other gas sensing.